A Regional Climatology of Monsoonal Precipitation in the Southwestern United States Using TRMM

CHRISTINA L. WALL, EDWARD J. ZIPSER, AND CHUNTAO LIU

University of Utah, Salt Lake City, Utah

(Manuscript received 17 March 2011, in final form 22 June 2011)

ABSTRACT

Using 13 yr of data from the Tropical Rainfall Measuring Mission (TRMM) satellite, a regional climatology of monsoonal precipitation is created for portions of the southwest United States. The climatology created using precipitation features defined from the TRMM precipitation radar (PR) shows that the population of features includes a large number of small, weak features that do not produce much rain and are very shallow. A lesser percentage of large, stronger features contributes most of the region's rainfall. Dividing the features into categories based on the median values of volumetric rainfall and maximum height of the 30-dBZ echo is a useful way to visualize the population of features, and the categories selected reflect the life cycle of monsoonal convection. An examination of the top rain-producing features at different elevations reveals that extreme features tend to occur at lower elevations later in the day. A comparison with the region studied in the North American Monsoon Experiment (NAME) shows that similar diurnal patterns occur in the Sierra Madre Occidental region of Mexico. The population of precipitation features in both regions is similar, with the NAME region producing slightly larger precipitation systems on average than the southwest United States. Both regions on occasion demonstrate the pattern of convection initiating at high elevations and moving downslope while growing upscale through the afternoon and evening; however, there are also days on which convection remains over the high terrain.

1. Introduction

The North American monsoon (NAM) is a seasonal phenomenon that affects much of Mexico and the southwestern United States (Adams and Comrie 1997). The onset of the monsoon, which occurs around the second week of May for the highest peaks of the Sierra Madre Occidental (SMO) (Liebmann et al. 2008) and from late June to mid-July in Arizona (Carleton 1985), drastically changes weather conditions in affected areas by bringing rain and thunderstorms almost daily.

Precipitation during the monsoon exhibits a distinct diurnal cycle, which has been explored in detail in many previous studies (Adams and Comrie 1997; Balling and Brazel 1987; Brenner 1974; Maddox et al. 1995). Nearly every day, the elevated terrain of the Arizona and New Mexico (AZNM) region—including the Kaibab Plateau, the Mogollon Rim, the White Mountains, and mountains in southeast Arizona—experience late-morning-to-early-afternoon development of convection (Brenner 1974; Maddox et al. 1995). Later in the day the highest frequency of precipitation progresses from the highest terrain to the low deserts to the southwest (Balling and Brazel 1987; Maddox et al. 1995).

Terrain is an important factor influencing the development of convection during the monsoon, but remote regions of high terrain create difficulties in accurately describing this convection because of a limited number of ground-based observations. The use of satellites, especially the Tropical Rainfall Measuring Mission (TRMM), allows the creation of a database of monsoonal precipitation over the AZNM region that can characterize these features in new ways. Most importantly, the TRMM precipitation radar (PR) observes the vertical structure of precipitation over the entire domain. Thus, one objective of this paper is to use the unique viewing properties of the TRMM satellite to characterize the climatology of monsoonal precipitation features in the AZNM region in a quantitative manner in terms of mean size and area characteristics and the diurnal cycle. The characteristics of the general population of precipitation features can then be utilized as

Corresponding author address: Christina Wall, 135 S 1460 E, Room 806B, Salt Lake City, UT 84112.
E-mail: christy.wall@utah.edu

DOI: 10.1175/JHM-D-11-031.1

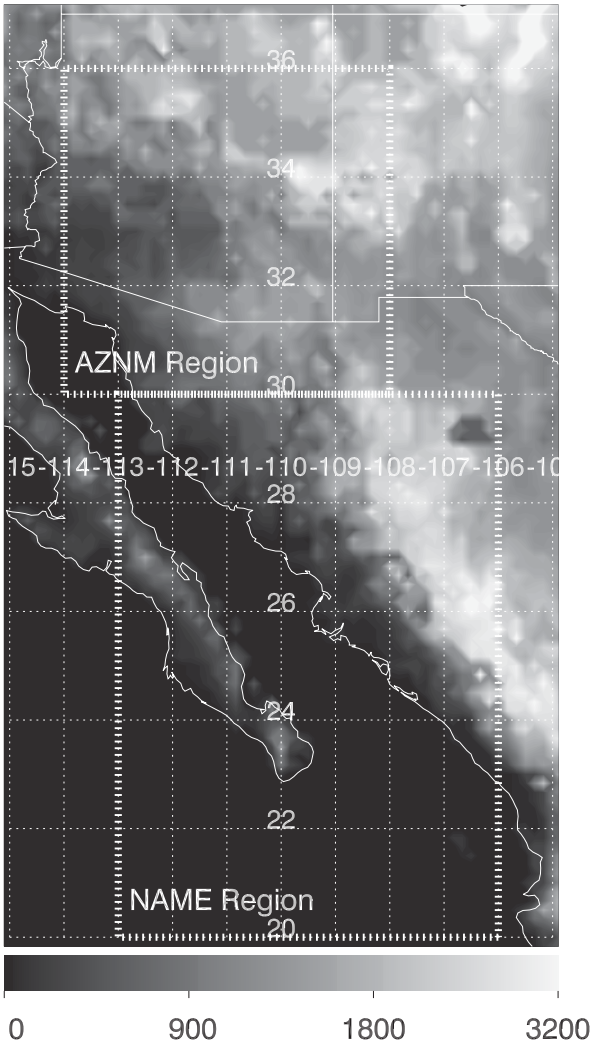

FIG. 1. Terrain height (m) within the regions of interest, which are denoted by the white boxes.

a framework to identify ''extreme'' precipitation features, which can result in devastating flash flooding in the region. The second objective of this paper is to examine the diurnal cycle of these extreme precipitation events by elevation.

The diurnal cycle of monsoonal convection in western Mexico, which is closer to the heart of the North American monsoon, has been described in great detail after the North American Monsoon Experiment (NAME), which took place in 2004 (Becker and Berbery 2008; Lang et al. 2007; Nesbitt et al. 2008; Rowe et al. 2008, 2011). Figure 1 shows a terrain map of both the AZNM and NAME regions. Terrain in the NAME region is dominated by the SMO, which runs from northwest to southeast in a nearly straight line with a coastal plain of similar width for the majority of the length of the mountain range. The AZNM region, on the other hand, has more complex and diverse terrain with numerous mountain ranges and plateaus. The similarities and differences between these regions will be discussed in greater detail in the discussion section.

Nesbitt et al. (2008) developed a conceptual model for daily monsoonal convection in the NAME region that described shallow convection initiating over the SMO in the late morning and then moving west and growing upscale. Past research suggests that the AZNM region projects a similar pattern, in which lower elevations are typically the location of the most intense convective activity, rather than the adjacent mountains where most thunderstorms form (Balling and Brazel 1987; Brenner 1974; Dunn and Horel 1994). The third objective of this paper is to compare the diurnal cycle of precipitation in the southwest United States to that of the NAME region in an attempt to determine whether the Nesbitt et al. (2008) model of convection initiating at high terrain and moving downslope and strengthening through the day applies to the AZNM region.

2. Data and methods

Satellite data play a key role in observing storm systems in the more remote areas of Arizona and New Mexico because of the scarcity of surface-observing sites and blockage of radar beams by high terrain. Thirteen years of TRMM PR data compensate for its infrequent sampling in constructing climatological statistics.

TRMM data used in this study were obtained from the University of Utah precipitation feature database (Liu et al. 2008). Radar precipitation features (RPFs) are classified by contiguous 2A25 near-surface raining pixels (Iguchi et al. 2000). This study uses data from July and August of 1998 through 2010 inclusive, with much of August 2001 omitted because of the orbital boost of TRMM. The PF database defines properties of these individual events, including maximum height of the 20-, 30-, and 40-dBZ echoes; volumetric rainfall from the 2A25 algorithm; minimum polarization-corrected temperature (PCT) for 37 and 85 GHz as seen by the TRMM Microwave Imager (TMI); area of the RPF; and the geocenter location of the RPF. Only features with at least two pixels (approximately 35 km^2) were included in an attempt to limit noise. Lightning flash count is determined using the TRMM Lightning Imaging Sensor (LIS), which is a staring optical imager that identifies changes in radiances in the field of view (Christian et al. 1999). The minimum detectable flash rate of this sensor is approximately 0.7 flashes per minute (Boccippio et al. 2002).

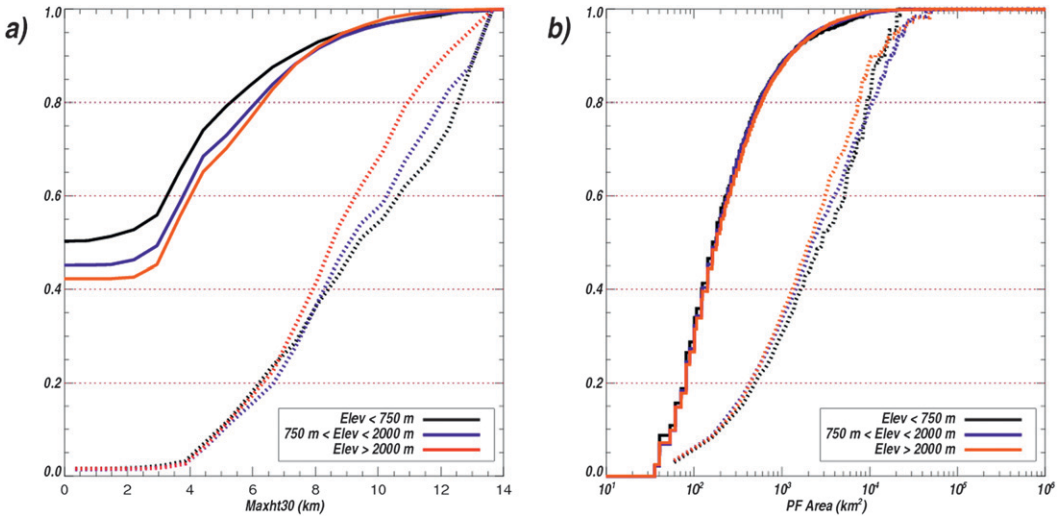

FIG. 2. Cumulative distribution functions of (a) the maximum height of the 30-dBZ reflectivity (solid lines) and (b) RPF area (solid lines). Rain contribution from these RPFs is shown with the dashed lines. Low elevations are represented by the black lines, middle elevations by the blue lines, and high elevations by the red lines.

To supplement TRMM's samples and include the evolution of monsoonal precipitation in the region, Next Generation Weather Radar (NEXRAD) radar data are compared to TRMM observations. The radar data utilized in this study are obtained from the National Climatic Data Center's NEXRAD Data Inventory Search. All available level 2 data from 1 July to 31 August 1999 are downloaded for both KFSX near Flagstaff and KEMX near Tucson, Arizona. Time resolution varied, ranging from 7 to 15 scans per hour. The National Center for Atmospheric Research (NCAR) program REORDER is used to transform the NEXRAD data from radar space to a Cartesian grid using a Cressman weighting function. The transformed data are interpolated to a grid centered on the radar site with 1-km resolution from −200 to 200 km in the x and y dimensions and 1-km resolution from 0 to 20 km in the z dimension. The radius of influence is 2 km in the x and y dimensions and 1 km in the z dimension. Every four points in the 1-km transformed NEXRAD data are then averaged to get a resolution of 4 km in the x and y dimensions so that the data can be comparable to TRMM PR data. On a pixel-by-pixel basis there is no significant bias in vertical reflectivity between the 4-km ground radar data and TRMM data. The degraded data are used to classify ground-based radar precipitation features (GPFs) similar to the RPFs categorized using TRMM. A GPF is defined as two or more contiguous pixels with a reflectivity of at least 15 dBZ at a level 3 km above the radar site in the transformed, degraded data. The default 88D Z–R relationship ($Z = 300R^{1.4}$) was used to calculate the rainfall rate at the 3-km level (Hunter 1996). The 3-km level is chosen based on properties of the beam in order to see the greatest range possible without being too high above the surface. One concern regarding this selection is that KFSX is located at an elevation of 2261 m, meaning that the level used to select GPFs is 5.2 km above sea level, implying that some features may be defined at bright band level. GPFs with an area of less than 35 km^2 are not included. The GPFs in this study are not identical to RPFs that would be seen by TRMM, but they fulfill the purpose of a comparison to ensure that the TRMM statistics are representative, despite a lack of time continuity.

3. Properties of monsoonal convection

The TRMM PF database includes over 100 000 RPFs within the AZNM region. This study examines July and August because these months are influenced primarily by the monsoon, unlike June or September, which are more likely to have outside synoptic influences. The region is divided arbitrarily into three elevation regimes relative to the height of the terrain features of interest: high, with elevation greater than or equal to 2000 m; middle, with elevation between 750 and 2000 m; and low, with elevation below 750 m. These categories are similar to those utilized by Nesbitt et al. (2008) and Rowe et al. (2008) to examine the NAME region so that comparisons can be made between the regions.

a. Using 30 dBZ as a threshold for features

Figure 2 shows cumulative distribution frequency (CDF) diagrams of the maximum height of the 30-dBZ

TABLE 1. Mean convective properties of RPFs in AZNM by centroid elevation.

Property	High elevations (>2000 m)	Middle elevations (750–2000 m)	Low elevations (<750 m)
Number of RPFs	3208	10 243	1622
Mean area of the RPFs (km^2)	625	645	661
Mean area of the top 20 RPFs (by rain volume) (km^2)	14 587	22 562	11 825
Mean rain volume of the top 20 RPFs (by rain volume) (km^2)	64 713	111 238	47 424
RPFs with at least one flash (%)	16.1	16.2	15.3
Volumetric rain from RPFs with at least one flash (%)	61.7	64.4	66.9
RPFs with more than five flashes (%)	6.5	7.2	7.9
Volumetric rain from RPFs with at least five flashes (%)	43.4	48.6	52.7

echo anywhere within the RPF and the RPF area. Nearly 50% of the population of RPFs in the region do not reach 30 dB*Z*, but of those that do, the vast majority have 30-dB*Z* echo extending only to 4–6 km. Higher elevations see a slightly higher percentage of features with 30-dB*Z* echo tops above 10 km, but these RPFs produce a smaller percent of the total rainfall at higher elevations than at middle or lower elevations. The shallow, weak RPFs that do not reach 30 dB*Z* tend to be very small, with over 80% having an area of less than 200 km^2 (not shown). Because these features contribute less than 2% of the region's rainfall, they are excluded from the remainder of the study.

b. *RPF area*

Figure 2b shows a CDF of RPF area for RPFs meeting the 30-dB*Z* threshold. Very little difference is seen in the areas for each elevation range—each elevation range is dominated by small-to-medium-sized features with areas less than 1000 km^2. Differences in rain contribution are not significant for small features, but on the larger end of the spectrum, the high and middle elevations derive slightly more rain from the very largest features. The largest 5% of features produce just over 40% of the total volumetric rainfall at all elevation ranges. It is important to note that the sample size decreases for these larger RPFs. Table 1 describes the mean properties of RPFs in AZNM with a 30-dB*Z* echo and sheds light on the larger features. Although each elevation regime has a similar value for mean RPF area, the mean area and rain volumes of the top 20 features (by volumetric rainfall) are largest for the middle-elevation category.

c. *Fraction of rain falling in small versus large and shallow versus tall features*

RPF size is closely tied to volumetric rainfall, although the relationship is not one to one. Figure 3 depicts the relationship between the maximum height of the 30-dB*Z* echo and rain volume for RPFs in AZNM. Features with higher 30-dB*Z* echo tops tend to produce larger volumes of rain. The color contours represent the TRMM RPFs defined using the PF database, and the black contours represent the population of GPFs defined using Flagstaff NEXRAD radar data (KFSX) from July and August 1999. The features defined using ground-based radar are not temporally restricted like the TRMM RPFs, although only two scans per hour were used to identify GPFs in order to increase the independence of each sample. The two-dimensional histograms match closely except for low values of rain volume, where the Flagstaff radar shows higher 30-dB*Z* echo tops than TRMM. This difference is caused by nonuniform beam filling and vertical beam spreading at large distances from the ground radar. When the distance of the center of the GPF is restricted to less than 90 km from the radar location, these features disappear and the populations look nearly identical. While there are many difficulties in comparing these two very different datasets, the similarities in the population of precipitation features from 13 yr of TRMM data and one summer of NEXRAD data are encouraging.

Using the two-dimensional histogram in Fig. 3, TRMM RPFs are subdivided into four intensity/size categories based on the median values of rain volume and maximum height of the 30-dB*Z* echo, which are 590 km^2 mm h^{-1} and 5.75 km, respectively. Features with a rain volume less than 590 km^2 mm h^{-1} are called ''small,'' and features with a rain volume larger than this number are called ''large.'' Features with the tallest 30-dB*Z* echo less than 5.75 km are called ''shallow,'' while features with higher maximum heights of 30 dB*Z* are labeled ''tall.'' These labels are then combined to form four categories in which the first term describes the height of the feature and the second characterizes the rain volume—shallow/small, tall/small, tall/large, and shallow/large. These categories and the numbers used to delineate them are subjective and relative to the population at hand.

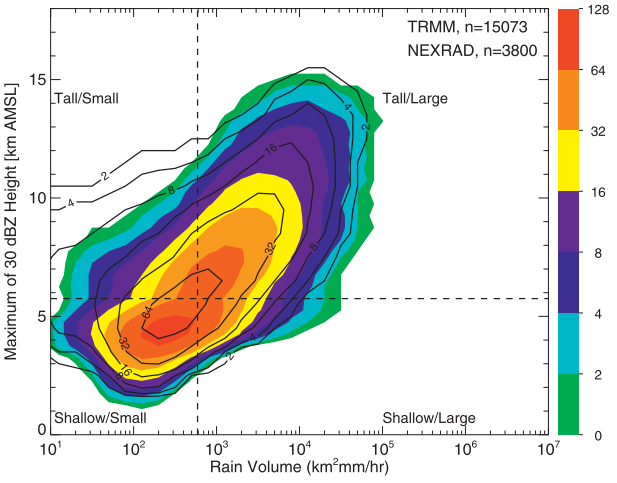

FIG. 3. Population of RPFs by volumetric rainfall and maximum height of the 30-dBZ echo is shown in colored contours. Black lines using the same contour intervals show a similar population of features defined using ground-based NEXRAD data from Flagstaff from July and August 1999. Median values of rain volume and maximum height of the 30-dBZ echo using TRMM RPFs are indicated by the black, dashed lines.

These categories reflect the life cycle of monsoonal convection in this area. Tall/small features are often developing convection and tall/large represents the mature phase of thunderstorms, while shallow/large corresponds to weakening thunderstorms or mesoscale convective systems with a large percentage of stratiform area. This concept is supported by the population of features in each category with lightning as shown in Table 2. The percentage of features in the tall/large category with at least one observed flash is an order of magnitude larger than values for the three other categories. It is likely that some flashes are missed in the other categories because their flash rates do not exceed one flash per minute.

A comparison of the percentages of shallow/large and tall/small features in each elevation regime reveals that tall features are more likely to occur at higher elevations, while shallow features are more likely to occur at low elevations. Based on our hypothesis of categories representing the life cycle of monsoonal convection, this would agree with studies that describe convection developing over high terrain and then moving into lower-elevation areas (Balling and Brazel 1987; Maddox et al. 1995).

d. Lightning flash rate

Lightning flash count observations differ only slightly between elevation ranges. Less than 20% of RPFs have one or more observed flashes. This is consistent with Fig. 3, which shows that the majority of RPFs do not have a 30-dBZ echo reaching above 6–7 km. The 20% of features with at least one flash produce around 65% of the region's volumetric rainfall (Table 1). Each elevation range has fewer than 8% of RPFs with more than five flashes, but these features produce nearly half of the region's volumetric rainfall. The more intense RPFs, which contribute greatly to the region's rain totals, are more likely to have lightning, although smaller or weaker features might have infrequent lightning that goes undetected, because flash rates of less than about one flash per minute are not detectable by TRMM (Boccippio et al. 2002).

4. Diurnal cycle of monsoonal convection

Monsoonal convection in AZNM has a distinct diurnal cycle similar to that in other mountainous areas of the world. The amount of rain falling at high and middle elevations increases sharply at 1000 local standard time (LST), as seen in Fig. 4. Middle elevations have a later but distinct peak at 1400 LST, after which time precipitation begins to drop off. Lower elevations show an even later, broader peak and do not demonstrate as much of a diurnal cycle. These results are consistent with the findings of Hirose and Nakamura (2005), who examined precipitation over the Tibetan Plateau. The number of features (not shown) at high and middle elevations begins to increase after 1000 LST—the time at which the number of small systems begins to increase on the Tibetan Plateau (Hirose and Nakamura 2005) and deeper clouds and self-sustaining circulation begins to develop in Colorado thunderstorms (Banta and Schaaf 1987).

The amount of rain falling from small/tall and small/shallow features begins to increase at around 1000 LST

TABLE 2. Characteristics of TRMM RPFs in difference intensity/size categories.

	Shallow/small	Shallow/large	Tall/small	Tall/large
Total % of features	40.4	10.5	9.6	39.5
% of total volumetric rain	3.6	7.8	1.2	87.4
Features with at least one flash (%)	1.6	5.1	8.0	56.0
Features with centroid elevation $>$ 2000 m (%)	38.6	9.6	11.2	40.6
Features with 750 m $<$ centroid elevation $<$ 2000 m (%)	40.0	10.6	9.3	40.1
Features with centroid elevation $<$ 750 m (%)	46.8	11.2	8.3	33.7

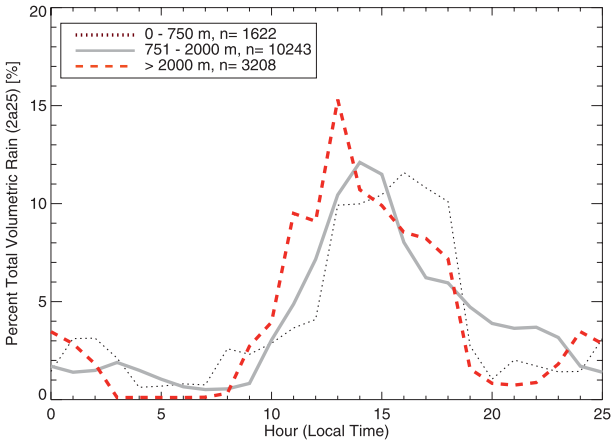

FIG. 4. Diurnal cycle of rainfall for the three different elevation categories based on the 3-h running mean of hourly contribution to total rainfall in each elevation regime in the region of interest. Low elevations are represented by the black dotted line, middle elevations by the solid gray line, and high elevations by the red dashed line.

(Fig. 5). The peak in the tall/large category lags the small RPFs by two hours, and the shallow/large features have a much later peak, which is consistent with the hypothesis that these categories represent stages in the convective life cycle. This pattern is substantiated by NEXRAD radar loops of monsoon days in the southwest United States such as the one shown in Fig. 6.

5. Example of monsoonal convection seen with TRMM

Figure 6 shows the evolution of an example of intense monsoonal convection that occurred on 25–26 July 2006. It begins as a few small thunderstorms over the northwest–southeast oriented high terrain of the Mogollon Rim shortly after 1200 LST. The coverage of precipitation grows, and by 1930 LST, a mesoscale convective system (MCS) with a linear leading edge is progressing from higher terrain into the middle-elevation range. A large area of stratiform rain develops behind this MCS as it moves to the southwest. Figure 7 shows a TRMM cross section of this feature (denoted by the black line in the third panel of Fig. 6), which falls into the tall/large category and ranks eighth out of all features in the region in terms of maximum height of the 30-dBZ reflectivity, which exceeds 15 km. This clearly places this feature in the top 1% of RPFs seen in Fig. 2. Over 150 flashes are observed within this system during the TRMM overpass. This feature is also one of the top 10 RPFs based on amount of volumetric rainfall. The 37- and 85-GHz PCTs show significant depressions over the core of the MCS, indicating large ice particles aloft (for a discussion of this parameter and its uses, see Spencer et al. 1989 and Mohr and Zipser 1996).This case is an example of convection initiating over the high terrain and growing upscale into a large MCS as it moves downslope toward lower elevations.

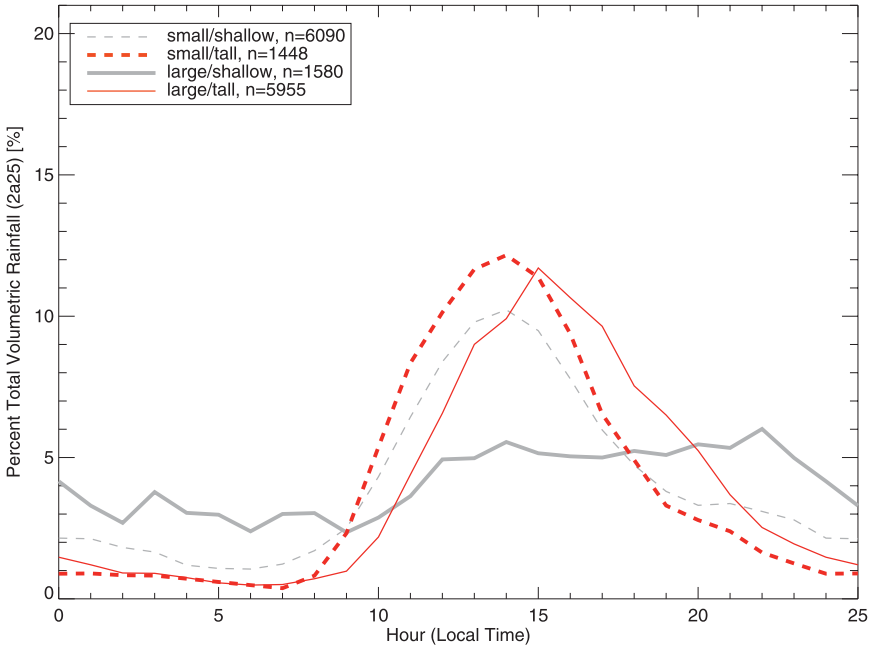

FIG. 5. Diurnal cycle of rainfall for the four categories of precipitation features identified in Fig. 3 based on the 3-h running mean of hourly contribution to total rainfall in the region of interest.

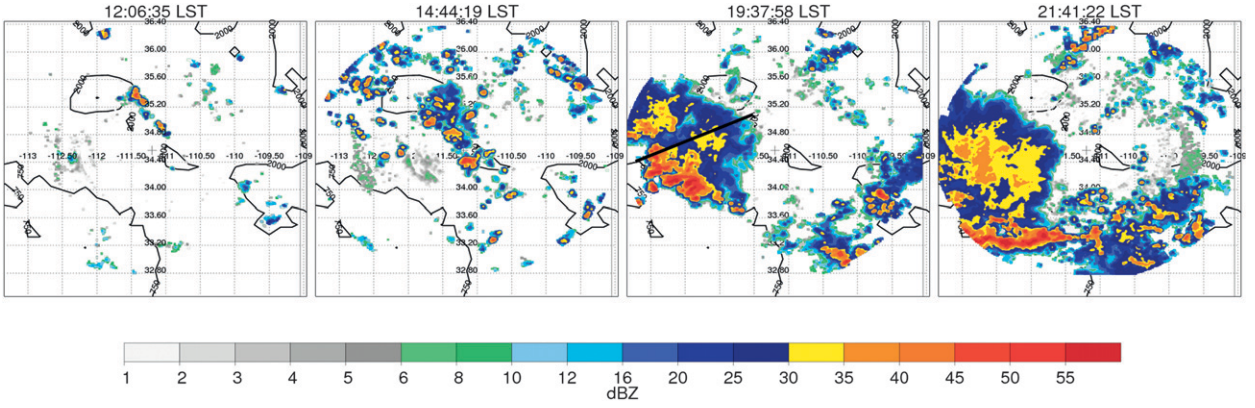

FIG. 6. A radar time series from KFSX NEXRAD on 25–26 Jul 2006. The line in the third panel indicates the location of the TRMM cross section shown in Fig. 7.

6. Comparison with the NAME region

The basic premise of the Nesbitt et al. (2008) model of convection in the NAME region is that upscale development of small features over the high terrain into larger convective systems such as that shown in section 5 is common, allowing for a comparison of its relative frequency between the AZNM and NAME regions. In the NAME region, precipitation initiates and often completes its life cycle earlier over the high terrain of the SMO (Becker and Berbery 2008). This convection over the high terrain tends to be shallower with lower rainfall intensity (Nesbitt et al. 2008; Rowe et al. 2008, 2011). Peak precipitation rates occur over the western foothills of the SMO as convection moves down the slope and increases in strength (Becker and Berbery 2008; Lang et al. 2007; Rowe et al. 2011). Occasionally these features persist into the early morning hours as MCSs over the Gulf of California (Lang et al. 2007; Nesbitt et al. 2008). The data used in studies of the NAME region are based on polarimetric radar data that was collected during the 2004 field campaign. The TRMM PF database can be used to compare this year to the 13-yr climatology of RPFs, as well as provide a consistent basis of comparison with the AZNM region.

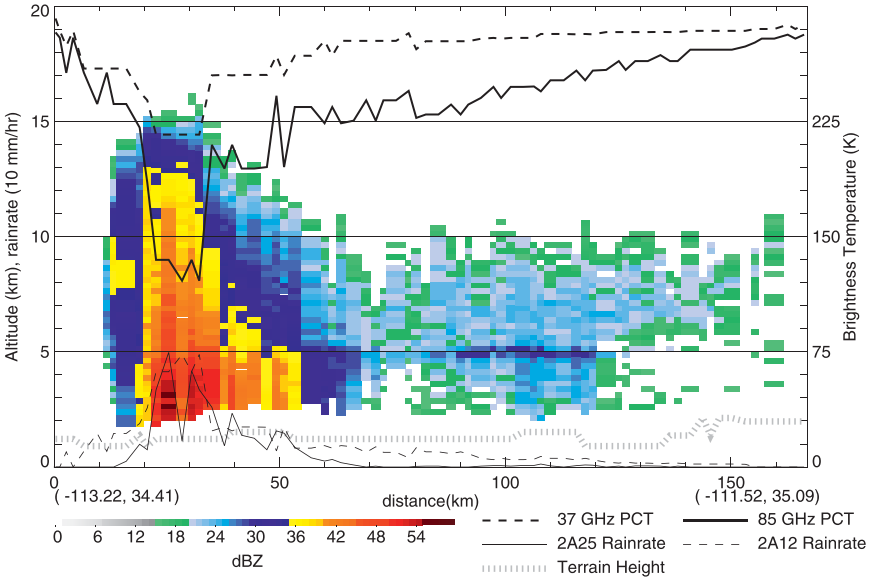

FIG. 7. TRMM overpass of the line of thunderstorms between Flagstaff and Phoenix on 26 Jul 2006. At the top of the figure the solid line indicates minimum 85-GHz PCT and the dashed line shows 37-GHz PCT. On the bottom of the figure, the gray short dashed line shows terrain height in km, the solid line shows rain rate from the 2A25 algorithm, and the black long dashed line shows rain rate from the 2A12 algorithm.

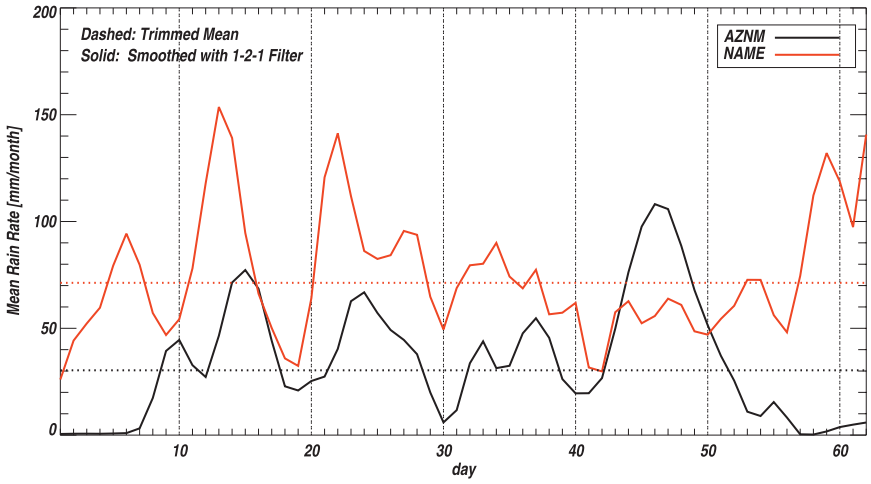

FIG. 8. 3B42 mean rain rates for the AZNM (black) and NAME (red) regions for the months of July and August 2004.

Figure 8 shows the daily mean rain rate from the 3B42 product for both regions for the 2004 year. This algorithm is gauge corrected (Huffman et al. 2007). The dashed lines show the long-term mean rain rate for July and August for both regions. The mean daily rain rate for the NAME region is more than twice that for AZNM, and NAME rainfall starts earlier in July and continues past the end of August. The NAME region receives more rainfall than the AZNM region for almost the entire two months, derived from a combination of the greater number of precipitation features and larger areal extent of features (Tables 1 and 3; see discussion below).

To compare the daily evolution of precipitation in the AZNM and NAME regions, a dataset of RPFs is selected from the NAME region. Only RPFs over land were used. By using the same data source and selection criteria for both regions, we achieve a more direct comparison than by comparing TRMM RPFs in AZNM to ground-based radar data in the NAME region. Comparisons of minimum IR temperature per feature and the maximum height of the 20-dBZ reflectivity per feature show similar patterns, but only a few of these figures are included for brevity (Figs. 9–11). Please note that in the AZNM figures, the 2000-m elevation is contoured; however, in the NAME region, 2250 m is contoured so that the results are directly comparable to Nesbitt et al. (2008). These elevation ranges were chosen based on the height of the terrain features of interest.

Figure 9 shows the increase in the number of RPFs with 20-dBZ echo tops from 6 to 10 km in the early afternoon. In the NAME region, the diurnal pattern of convection initiating over the high terrain and moving westward is visible—the number of shallow features over the high terrain peaks between 14 and 16 LST. Between 16 and 18 LST, the peak moves to the west over the slopes of the SMO. The AZNM clearly shows an increase in the frequency of RPFs during the afternoon,

TABLE 3. Mean convective properties of RPFs in the NAME region.

Property	High elevations (>2250 m)	Middle elevations (500–2000 m)	Low elevations (<500 m)
Number of RPFs	2068	10 192	2379
Mean area of the RPFs (km^2)	783	742	858
Mean area of the top 20 RPFs (by rain volume) (km^2)	20 448	30 184	25 977
Mean rain volume of the top 20 RPFs (by rain volume) (km^2)	82 551	144 865	119 598
RPFs with at least one flash (%)	11.6	13.5	14.4
Volumetric rain from RPFs with at least one flash (%)	60.0	65.2	69.4
RPFs with more than five flashes (%)	4.8	6.2	8.2
Volumetric rain from RPFs with at least five flashes (%)	40.2	49.6	57.2

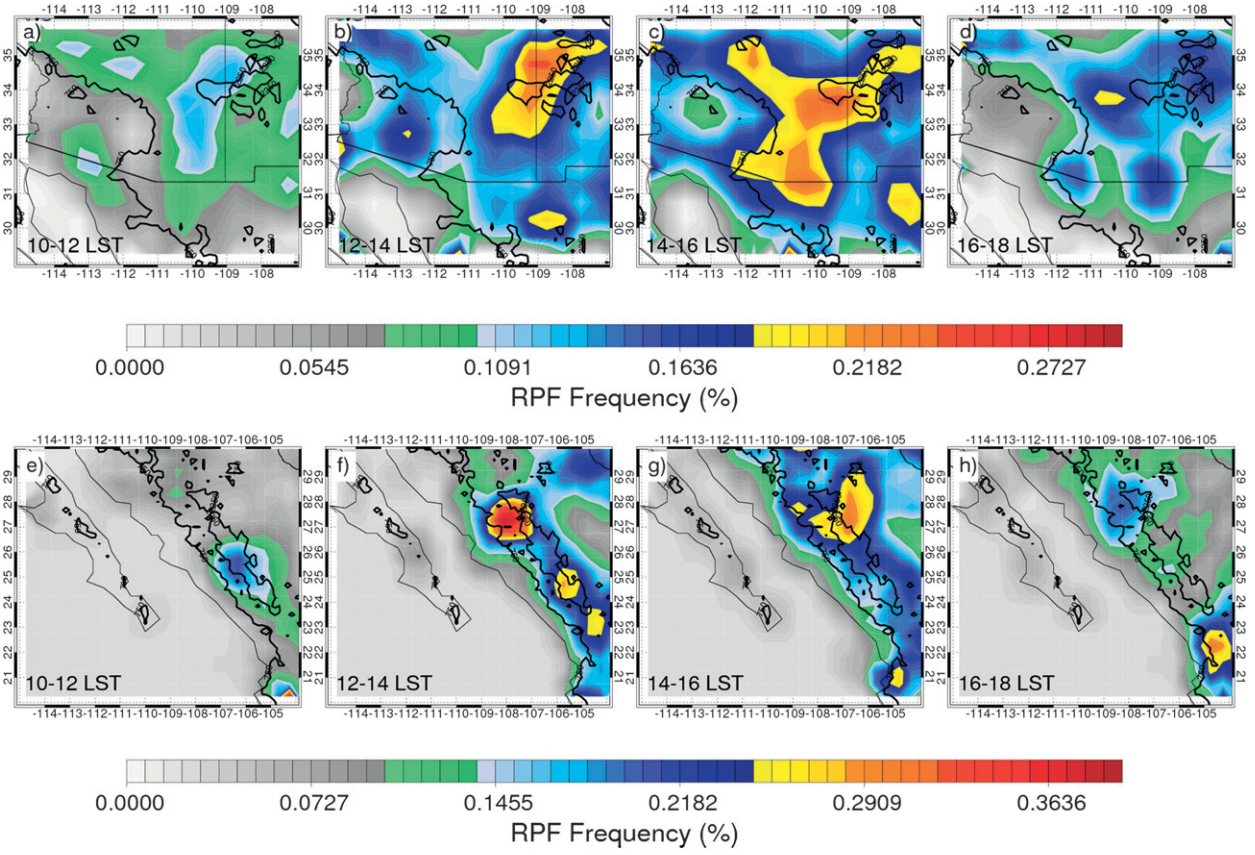

FIG. 9. The diurnal cycle of RPFs in the AZNM and NAME regions as shown by the frequency of RPFs (contoured in color) with areas larger than 100 km^2 in the (a)–(d) AZNM and (e)–(h) NAME regions. The time is noted in the lower left corner. All of these features have 20 dBZ reflectivity between 6 and 10 km. This has been corrected for TRMM orbital sampling bias. The heavy black lines show the 750- and 2000-m contours for AZNM and 750- and 2250-m contours for NAME.

but shallow features occur over the high terrain all evening, and no westward movement is visible.

What about deeper features? Figure 10 shows the locations of RPFs larger than 100 km^2 with 20-dBZ echo tops ranging from 12 to 14 km. As with the 8–10-km features, the number of RPFs increases rapidly in early afternoon. There are more RPFs at high elevations in the SMO from 12 to 14 LST, and the number of features along the western slopes increases during the afternoon, but RPFs still occur at high elevations in late afternoon. A similar pattern is observed in AZNM, where features with 20-dBZ echo tops between 12 and 14 km are located preferentially over areas of higher terrain between 10 and 12 LST. Despite increasing in number over the lower elevations in the afternoon, RPFs occur over the highest terrain at all hours.

Figure 11 shows the diurnal cycle of more intense RPFs, with area larger than 100 km^2 and 20-dBZ echo tops above 14 km. In both regions a large increase in the number of these features occurs over high terrain from 10–12 LST to 12–14 LST. Later in the afternoon, more of these strong RPFs occur at lower elevations, but there are still features occurring over the high terrain, particularly in the AZNM region. The only difference in the two regions occurs at 16–18 LST when the majority of the strong features in the NAME region are occurring over the western foothills of the SMO, rather than over both foothills and high peaks as in AZNM.

A closer examination of the diurnal cycle of the 50 most extreme precipitation events (Figs. 12 and 13) in both regions demonstrates that the rainiest features do exhibit a pattern of downslope motion during the afternoon. High elevations in AZNM show a broad peak beginning from 12 to 14 LST, while the middle elevations peak from 16 to 18 LST, and low elevations have a peak from 16 to 22 LST. In the NAME region, high elevations peak from 14 to 16 LST, while middle elevations have a much later peak from 22 to 24 LST. Low elevations have a peak at 18–20 LST as well as 00–02 LST. The peaks in each elevation regime occur earlier in AZNM than in the NAME region. Based on the top 50 features from the last 13 yr, high-rain-producing events are more likely to occur earlier in the day at

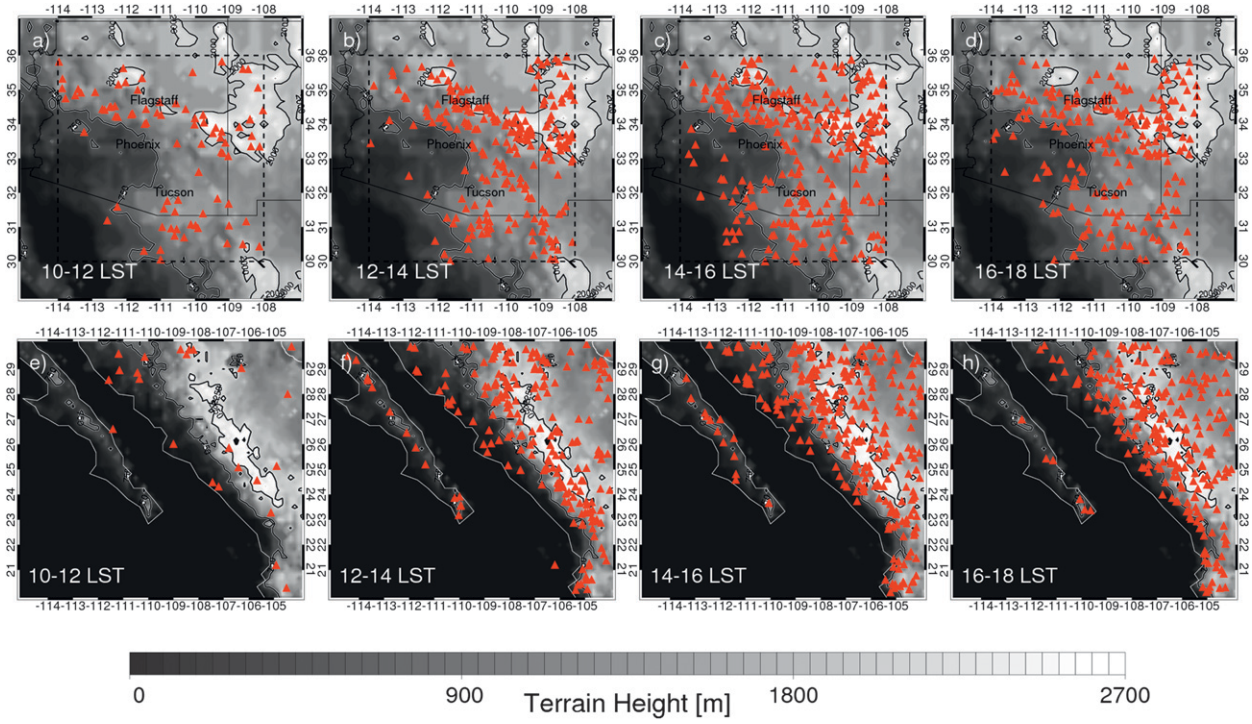

FIG. 10. The diurnal cycle of RPFs in the AZNM and NAME regions as shown by the locations of RPFs (red triangles) with areas larger than 100 km^2 in the (a)–(d) AZNM and (e)–(h) NAME regions. The time is noted in the lower left corner. All of these features have 20-dBZ reflectivity between 12 and 14 km. The high elevation regime is contoured by the heavy black line.

higher elevations and later in the day at low elevations, as suggested by Nesbitt et al. (2008).

The centroid is not always the most accurate measure of RPF location, especially with larger features. Figure 14 shows the diurnal cycle of rainfall from 13 yr of TRMM PR data in July and August at 0.1° resolution. The highest rainfall rates occur between 15 and 18 LST in the foothills just west of the SMO. Earlier in the day precipitation tends to occur over the high terrain, particularly along the Mogollon Rim in AZNM. Precipitation is still occurring over the high terrain from 18 to 21 LST, but the overall pattern agrees with the model of Nesbitt et al. (2008). While TRMM data shows examples of deep convection occurring over the higher terrain of the SMO later in the afternoon and early evening, it clearly does not contribute a great amount of rainfall to the region's precipitation.

Tables 1 and 3 provide a quantitative comparison between RPFs occurring in different elevation ranges for the AZNM and NAME regions. RPFs in the NAME region have a larger mean area. Additionally, the top 20 RPFs (by rain volume) have greater mean areas and rain volumes than the top 20 RPFs in the AZNM region. More features in AZNM have observed lightning, but features with lightning produce around 60% of each region's volumetric rainfall. Aside from the area of the largest features and the percentage of features with lightning, the RPFs in these regions are comparable.

7. Discussion

The AZNM and NAME regions have similarities and differences in both the regional RPFs and characteristics that affect these RPFs, such as terrain and moisture availability. The 13-yr climatology of RPFs from the TRMM precipitation feature database shows that the populations of features in both regions are similar. On average the NAME region produces larger and rainier RPFs. The diurnal cycles of all but the most intense features are nearly identical for both regions, with monsoonal features initiating over the higher terrain around local noon. During the afternoon, the number of RPFs increases, and precipitation develops over the middle and lower elevations. In the NAME region, fewer intense RPFs occur over the highest terrain of the SMO late in the day, while in AZNM intense RPFs can occur over high terrain all afternoon.

Many previous studies have discussed convection initiating over the SMO and growing upscale and moving downslope during the afternoon (Lang et al. 2007; Nesbitt et al. 2008; Rowe et al. 2008, 2011). While this pattern describes the convection on most days, the

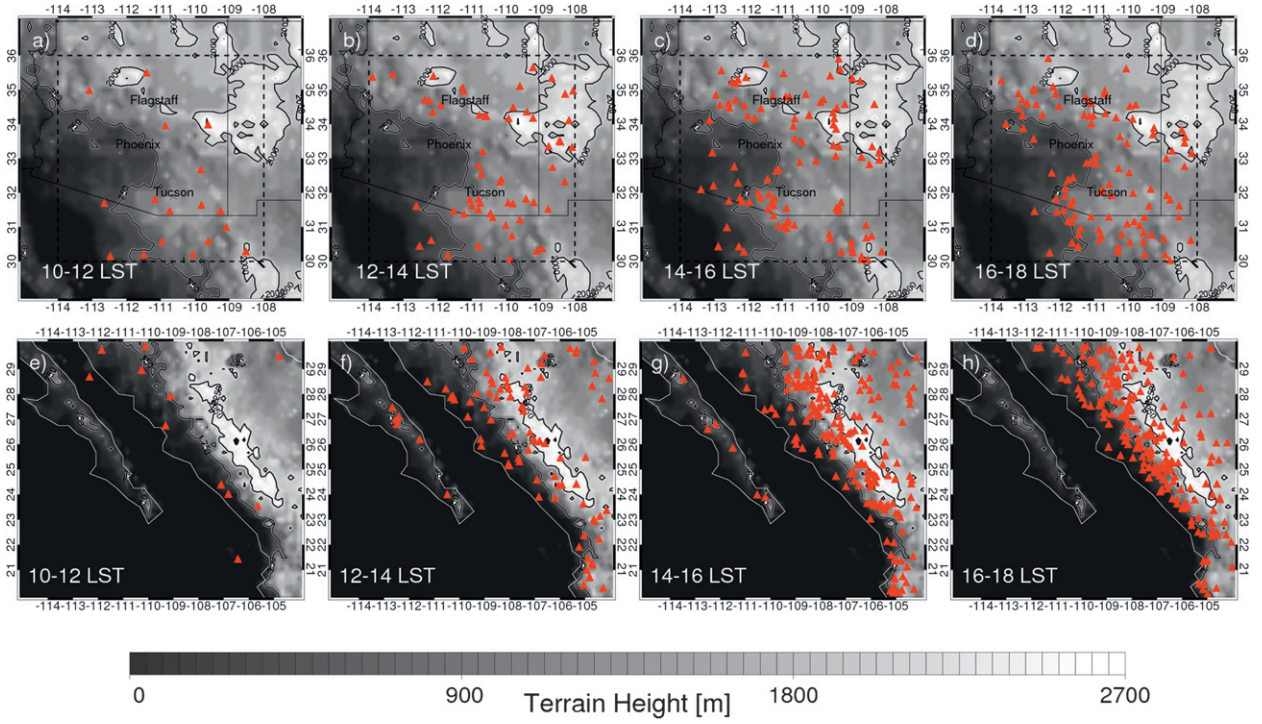

FIG. 11. The diurnal cycle of RPFs in the AZNM and NAME regions as shown by the locations of RPFs (red triangles) with areas larger than 100 km^2 in the (a)–(d) AZNM and (e)–(h) NAME regions. The time is noted in the lower left corner. All of these features have 20-dBZ reflectivity above 14 km.

13-yr climatology shown here demonstrates that there are days on which strong (20-dBZ echo tops occurring over 14 km) convection occurs on the higher terrain of the SMO as well as the high plateaus to the east in the late afternoon and early evening [it should be noted that this plateau was out of the range of the S-band dual-polarization Doppler radar (S-Pol) used for the previous NAME studies mentioned here]. Rowe et al. (2011) saw brief periods of intense rainfall at higher elevations in the NAME data and suggest that while there is deep convection over the SMO, the overall trend is consistent with the Nesbitt et al. (2008) model.

Lang et al. (2007) examined organized convective features in the context of different meteorological regimes and found that during disturbed periods, organized convective features tended to be located in the foothills of the

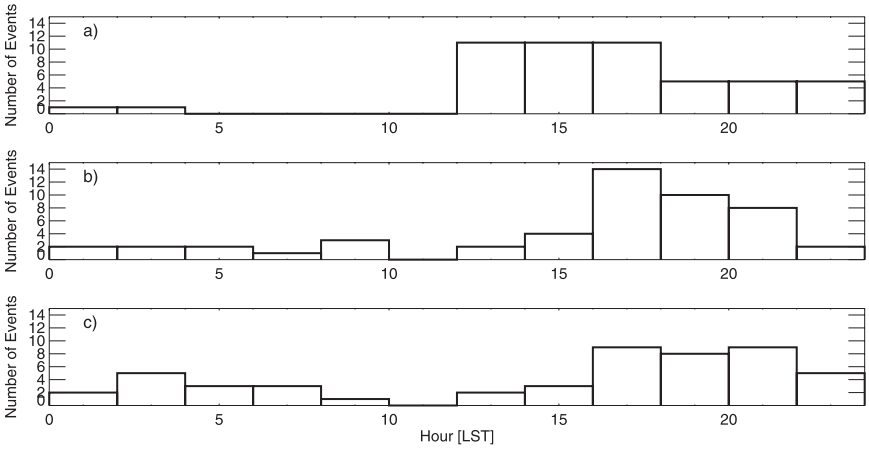

FIG. 12. Histogram of the time of occurrence of the top 50 RPFs in the AZNM region, as ranked by volumetric rainfall for (a) high-, (b) middle-, and (c) low-elevation regimes.

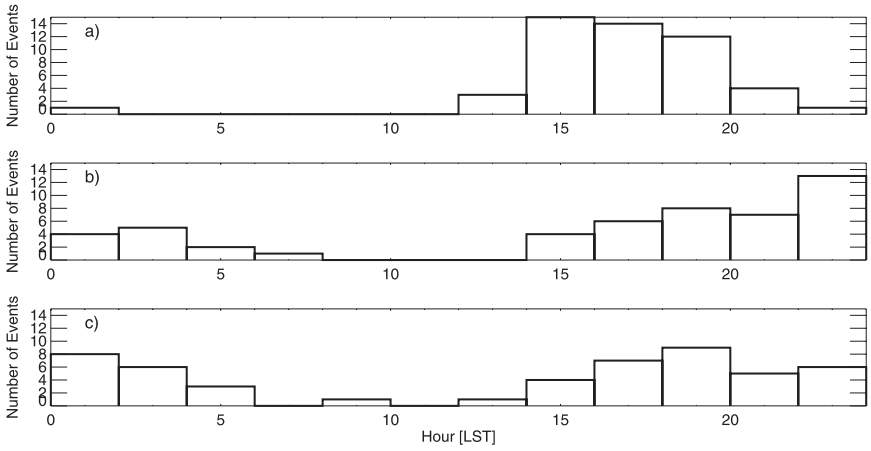

FIG. 13. Histogram of the time of occurrence of the top 50 RPFs in the NAME region, as ranked by volumetric rainfall for (a) high-, (b) middle-, and (c) low-elevation regimes.

SMO, while during "no regime" periods, organized features were confined to the higher terrain. This idea almost certainly applies to the AZNM region as well. Maddox et al. (1995) identifies several synoptic patterns during which severe thunderstorms tend to develop in Arizona. Other work (not shown) by the authors to identify "burst" and "break" periods in the AZNM region shows that the vast majority of large and intense storms in the TRMM database in this region occur during these burst periods, which have higher relative humidities in the lower troposphere. Time mean precipitable water values are nearly two times higher in the NAME region than in AZNM during the summer months (Berbery 2001, his Fig. 6; Higgins et al. 1997, their Fig. 10), suggesting that the NAME region has more total column moisture available.

Radar loops from Flagstaff show days when convection in AZNM remains isolated over the Mogollon Rim and days on which convection grows upscale and moves into lower terrain, as shown in the example in Figs. 6 and 7. It seems likely that the days on which convection moves downslope in AZNM would demonstrate similar characteristics to "disturbed" days in the NAME region.

The Mogollon Rim and the SMO are alike in that both are linear expanses of high terrain with foothills to the southwest and higher plateaus to the northeast. Regardless of the motion of convection along these features, other areas of higher terrain (in AZNM, the White Mountains and mountains in southern Arizona, and in NAME, the high plateau to the east of the SMO) continue to host RPFs all afternoon, with no signs of downslope motion. This can be observed to the northeast of Flagstaff in Fig. 6. Lang et al. (2007) points out that either a very shallow or extremely weak cold pool is sufficient to explain the propagation of convection off the SMO. Because the Mogollon Rim is similar in shape and elevation, similar dynamics are likely driving the downslope motion in the AZNM region. The diurnal cycle of extreme events shown in Figs. 12 and 13 depicts a downslope motion of the rainiest RPFs through the afternoon, so it seems likely that dynamics that support the upscale growth of small features into a larger convective system also support downslope motion from the high terrain into lower elevations. One of the principle differences between the two regions seems to be that the SMO has enough moisture and instability to sustain storms moving downslope more often than the AZNM region.

8. Conclusions

The properties of RPFs from the 13-yr climatology of the TRMM precipitation feature database described above demonstrate that only about 13% of RPFs are deep and large, but they are responsible for 87% of the rainfall. Many of these features occur over the high terrain of the Mogollon Rim, the Kaibab Plateau, and other mountain ranges. The majority of RPFs that occur in the southwest United States during the months of July and August are smaller and weaker. Radar loops from the NEXRAD radar at Flagstaff show that on some days, the shallow convection that initiates over the higher terrain of the Mogollon Rim and Kaibab Plateau (and frequently remains there) develops upscale into larger, deeper convective features that may move off of the high terrain and into lower elevations.

A comparison with the region observed during the NAME field campaign shows similar patterns. Nesbitt et al. (2008) describe a general model in which weak, shallow convection develops midday at the high elevations of the SMO and then moves downslope through the afternoon and evening, while growing in spatial scale

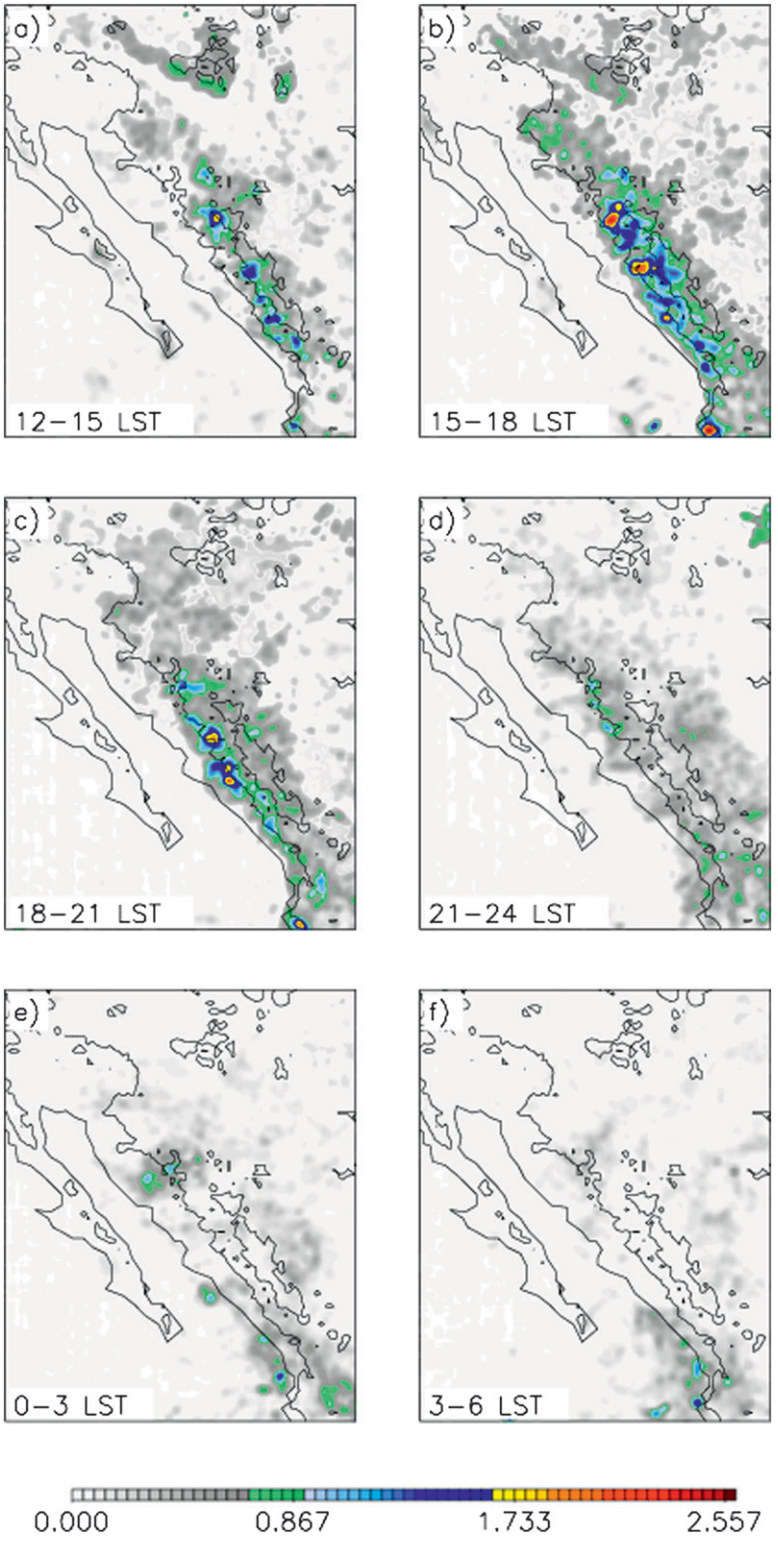

FIG. 14. Diurnal pattern of unconditional rainfall (mm h^{-1}, contoured in color) from 13 yr of TRMM PR data from July and August at 0.1° resolution from (a) 12 to 15, (b) 15 to 18, (c) 18 to 21, (d) 21 to 24, (e) 0 to 3, and (f) 3 to 6 LST. The black lines are the contours of the coast: 750 and 2250 m.

and intensity. While this pattern is appropriate for most days in both the AZNM and NAME regions, the TRMM data show that there are days on which tall convective features occur over the SMO–Mogollon Rim and other high terrain, as has been noted by Rowe et al. (2011) and Lang et al. (2007). Rainfall from the TRMM PR indicates that these features do not provide much of a contribution to rainfall in the region. The downslope motion of convection as described by Nesbitt et al. (2008) is more important to the hydrologic cycle.

The diurnal cycle of extremely rainy RPFs indicates that downslope motion is observed when stronger convection develops. Mean characteristics of the RPFs in both regions are surprisingly similar. The NAME region tends to produce slightly larger RPFs. The AZNM region has a slightly larger percentage of features with observed lightning, and it would be interesting to compare the microphysical characteristics of features with lightning in both regions.

While the regions have different physical characteristics, enough similarities exist to show that a more detailed comparison between intense cases in both regions would be worthwhile. A plethora of data was gathered during the NAME field campaign, and using this data to understand the mechanisms that cause stronger storms to move off the high terrain of the SMO may lead to a better understanding of the motions of intense, destructive convection off of the Mogollon Rim.

Acknowledgments. The authors thank Steve Nesbitt as well as the anonymous reviewers for their comments, which greatly improved the manuscript. Radar data were downloaded from the National Climatic Data Center (NCDC) at http://www.ncdc.noaa.gov/nexradinv/. This work was supported by National Aeronautics and Space Administration Grant NNX10AG90G.

REFERENCES

Adams, D. K., and A. C. Comrie, 1997: The North American monsoon. *Bull. Amer. Meteor. Soc.,* **78,** 2197–2213.

Balling, R. C., and S. W. Brazel, 1987: Diurnal variations in Arizona monsoon precipitation frequencies. *Mon. Wea. Rev.,* **115,** 342–346.

Banta, R. M., and C. B. Schaaf, 1987: Thunderstorm genesis zones in the Colorado Rocky Mountains as determined by traceback of geosynchronous satellite images. *Mon. Wea. Rev.,* **115,** 463–476.

Becker, E. J., and E. H. Berbery, 2008: The diurnal cycle of precipitation over the North American monsoon region during the NAME 2004 field campaign. *J. Climate,* **21,** 771–787.

Berbery, E. H., 2001: Mesoscale moisture analysis of the North American monsoon. *J. Climate,* **14,** 121–137.

Boccippio, D. J., W. J. Koshak, and R. J. Blakeslee, 2002: Performance assessment of the optical transient detector and lightning imaging sensor. Part I: Predicted diurnal variability. *J. Atmos. Oceanic Technol.,* **19,** 1318–1332.

Brenner, I. S., 1974: A surge of maritime tropical air—Gulf of California to the southwestern United States. *Mon. Wea. Rev.,* **102,** 375–389.

Carleton, A. M., 1985: Synoptic and satellite aspects of the southwestern U.S. summer 'monsoon'. *J. Climatol.,* **5,** 389–402.

Christian, H. J., and Coauthors, 1999: The Lightning Imaging Sensor. *Proc. 11th Int. Conf. on Atmospheric Electricity,* Huntsville, AL, NASA, 746–749.

Dunn, L. B., and J. D. Horel, 1994: Prediction of central Arizona convection. Part I: Evaluation of the NGM and Eta model precipitation forecasts. *Wea. Forecasting,* **9,** 495–507.

Higgins, R. W., Y. Yao, and X. L. Wang, 1997: Influence of the North American monsoon system on the U.S. summer precipitation regime. *J. Climate,* **10,** 2600–2622.

Hirose, M., and K. Nakamura, 2005: Spatial and diurnal variation of precipitation systems over Asia observed by the TRMM precipitation radar. *J. Geophys. Res.,* **110,** D05106, doi:10.1029/2004JD004815.

Huffman, G. R., and Coauthors, 2007: The TRMM multisatellite precipitation analysis (TMPA): Quasi-global, multiyear, combined-sensor precipitation estimates at fine scales. *J. Hydrometeor.,* **8,** 38–55.

Hunter, S. M., 1996: WSR-88D radar rainfall estimation: Capabilities, limitations and potential improvements. *Natl. Wea. Dig.,* **20,** 26–38.

Iguchi, T., T. Kozu, R. Meneghini, J. Awaka, and K. Okamoto, 2000: Rain-profiling algorithm for the TRMM precipitation radar. *J. Appl. Meteor.,* **39,** 2038–2052.

Lang, T. J., D. A. Ahijevych, S. W. Nesbitt, R. E. Carbone, S. A. Rutledge, and R. Cifelli, 2007: Radar-observed characteristics of precipitating systems during NAME 2004. *J. Climate,* **20,** 1713–1733.

Liebmann, B., I. Blade, N. A. Bond, D. Gochis, D. Allured, and G. T. Bates, 2008: Characteristics of North American summertime rainfall with emphasis on the monsoon. *J. Climate,* **21,** 1277–1294.

Liu, C., E. J. Zipser, D. J. Cecil, S. W. Nesbitt, and S. Sherwood, 2008: A cloud and precipitation feature database from nine years of TRMM observations. *J. Appl. Meteor. Climatol.,* **47,** 2712–2728.

Maddox, R. A., D. M. McCollum, and K. W. Howard, 1995: Large-scale patterns associated with severe summertime thunderstorms over central Arizona. *Wea. Forecasting,* **10,** 763–778.

Mohr, K. I., and E. J. Zipser, 1996: Defining mesoscale convective systems by their 85-GHz ice-scattering signatures. *Bull. Amer. Meteor. Soc.,* **77,** 1179–1189.

Nesbitt, S. W., D. J. Gochis, and T. J. Lang, 2008: The diurnal cycle of clouds and precipitation along the Sierra Madre Occidental observed during NAME-2004: Implications for warm season precipitation estimation in complex terrain. *J. Hydrol.,* **9,** 728–743.

Rowe, A. K., S. A. Rutledge, T. J. Lang, P. E. Ciesielski, and S. M. Saleeby, 2008: Elevation-dependent trends in precipitation observed during NAME. *Mon. Wea. Rev.,* **136,** 4962–4978.

——, ——, ——, 2011: Investigation of microphysical processes occurring in isolated convection during NAME. *Mon. Wea. Rev.,* **139,** 424–443.

Spencer, R. W., H. M. Goodman, and R. E. Hood, 1989: Precipitation retrieval over land and ocean with the SSM/I: Identification and characteristics of the ice scattering signal. *J. Atmos. Oceanic Technol.,* **6,** 254–273.